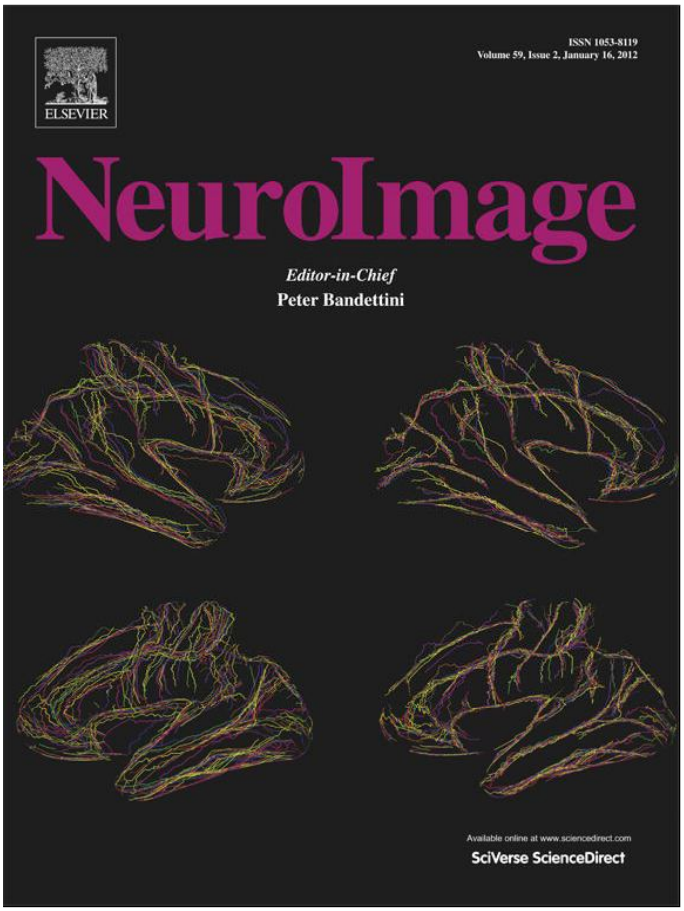

(This is a sample cover image for this issue. The actual cover is not yet available at this time.)

NeuroImage 59 (2012) 3347–3355

Contents lists available at SciVerse ScienceDirect

NeuroImage

journal homepage: www.elsevier.com/locate/ynimg

Investigating brain connectivity using mixed effects vector autoregressive models

Cristina Gorrostieta [a], Hernando Ombao [c,*], Patrick Bédard [b], Jerome N. Sanes [b]

[a] Department of Biostatistics, Brown University. 121 S. Main Street Providence, RI, 02912, USA
[b] Department of Neuroscience, Brown University, Providence, RI 02912, USA
[c] Department of Statistics, University of California, Irvine - Irvine, CA 92697, USA

ARTICLE INFO

Article history:
Received 19 April 2011
Revised 29 July 2011
Accepted 19 August 2011
Available online 6 October 2011

Keywords:
Vector auto-regressive (VAR) model
Linear mixed effects model
fMRI time series
Multi-subject
Brain effective connectivity

ABSTRACT

We propose a mixed-effects vector auto-regressive (ME-VAR) model for studying brain effective connectivity. One common approach to investigating inter-regional associations in brain activity is the multivariate auto-regressive (VAR) model. The standard VAR model unrealistically assumes the connectivity structure to be identical across all participants in a study and therefore, could yield misleading results. The ME-VAR model overcomes this limitation by incorporating a participant-specific connectivity structure. In addition, the ME-VAR models can capture connectivity differences across experimental conditions and patient groups. The ME-VAR model directly decomposes the connectivity matrices into (i.) the condition-specific connectivity matrix, which is shared by all participants in the study (fixed effect) and (ii.) a participant-specific component (random effect) which accounts for between-subject variation in connectivity. An advantage of our approach is that it permits the use of both theoretical results on mixed effects models and existing statistical software when fitting the model. Another advantage of the proposed approach is that it provides improved estimates of the within-subject coefficients (the random effects) by pooling information across subjects in a single-stage rather than the usual two-stage approach. We illustrate the ME-VAR model on a functional MRI data set obtained to investigate brain connectivity in the prefrontal, pre-motor and parietal cortices while humans performed a motor-related, decision-making and action selection task.

Introduction

Brain processes such as decision making and learning are mediated both via specific brain regions and inter-regional interactions (Fleming et al., 2010). Neuroimaging studies have revealed how various cognitive processes depend on cooperation between distinct brain regions (Albouy et al., 2008; Fleming et al., 2010). Moreover, several studies demonstrate that neurological disorders including schizophrenia, autism, epilepsy, and Parkinson's disease are not only characterized by specific neural impairments but also by whole-brain connectivity features that often correlate with disease status (Assaf et al., 2010; Benetti et al., 2009; Cadotte et al., 2009; Pollonini et al., 2010; Wu et al., 2010). These studies suggest that connectivity assessment is not only important to understanding the fundamental processes of the brain but also for characterizing some neurological diseases.

The goal in this paper is to develop a robust statistical model that describes effective connectivity between brain regions using functional MRI (fMRI) time-series data. This model will be utilized to: (i.) test for differences in brain connectivity across different experimental conditions; and (ii.) identify the specific temporal lags at which these differences exist. We will use the vector auto-regressive (VAR) model to characterize interactions between hemodynamic activity at different ROIs. Moreover, since it is important in multi-subject experiments to account for variation in brain connectivity patterns, we shall embed the VAR model in a mixed effects model framework. Our approach directly benefits from the theoretical advancements on mixed effects models and available statistical software for fitting the model.

One common approach to assess brain connectivity is by coherence and partial coherence analysis (see, e.g., Sun et al., 2004). These are model-free measures for testing linear associations between oscillatory activities at different brain regions. Coherence has an intuitive interpretation of being the squared cross-correlation between filtered time series recorded at different brain regions (see, e.g., Ombao and Van Bellegem, 2008 for a theoretical justification for this interpretation). However, the results of coherence analysis cannot differentiate between direct vs. indirect associations. By indirect association between ROIs, we refer to associations in brain hemodynamic activity between *A* and *B* that possibly may be mediated or controlled by another ROI *C*. In contrast, partial coherence measures direct linear associations between a pair of ROIs because it removes the linear effects of other ROIs in a network. Using partial coherence, one can assess connectivity both by the magnitude of partial coherence (which measures the strength of direct association) and the phase of coherency (which measures the time-

* Corresponding author. Fax: +1 401 863 9182.
E-mail address: hombao@uci.edu (H. Ombao).

1053-8119/$ – see front matter © 2011 Elsevier Inc. All rights reserved.
doi:10.1016/j.neuroimage.2011.08.115

lag between the two ROIs). However, there are major computational challenges to estimate partial coherence when the number of ROIs is large. To overcome these hurdles, Fiecas et al., 2010; Fiecas and Ombao, 2011 proposed a general spectral shrinkage method that is more accurate and stable than standard approaches, such as the multi-taper method. An attractive feature of this approach is that it is not constrained by any strict parametric form for connectivity and hence is immune to problems arising from mis-specifying a parametric model. Nevertheless, one can still encounter difficulties with this method in estimating lags (through the phase) with short time series. Moreover, this method does not easily integrate information on between-subject variation a weakness that is also shared by current implementations of multi-taper approaches.

Here, we propose to study brain effective connectivity using the vector auto-regressive (VAR) model. The VAR model has been applied to fMRI time series (e.g., Goebel et al., 2003; Harrison et al., 2003; Roebrock et al., 2005) and EEG data sets (e.g., Kaminski and Blinowska, 1991). The VAR model has achieved relatively wide acceptance since it provides a context for testing Granger causality, a common method used to assess between region effective connectivity that also suggests directionality of the connectivity (Roebrock et al., 2005; Goebel et al., 2003). Under the VAR model framework, it is also possible to provide a parametric approach to determine coherence, partial coherence and Granger causality in the frequency domain (Chen et al., 2009). Thus, VAR modeling presents a broad context for exploring connectivity between ROIs. Contrary to coherence, under the VAR model framework, short time series do not usually represent a problem in model fitting. Moreover, one can naturally include between subject variation by extending the VAR model to a mixed effects VAR model.

Nevertheless, the standard VAR model has limits insofar that, at least with current implementations, it does not include variation in connectivity across participants in a multi-subject study. One natural approach would be to proceed with the estimation of connectivity parameters in two stages: subject-specific parameters are estimated on the first stage and between-participant variation in the connectivity parameters is estimated in the second. This approach is also valid and at times necessary in situations where the data is massive and requires some level of dimension reduction by first computing subject-specific estimates. However, the two-stage approach is known in the statistical literature to be sub-optimal because information is lost when summarizing the original vector-valued time series for the s-th subject by its own connectivity parameter matrices. This limitation is true for any analysis based on "summary statistics" rather than the full data.

To overcome this limitation, we propose a generalization the usual VAR model by embedding it in the linear mixed effects framework. The mixed effects VAR model (ME-VAR) decomposes the connectivity matrices into (i.) the condition-specific connectivity matrix (fixed effect) and (ii.) a participant-specific component (random effect) to model between-participant variation in connectivity. This approach has a number of advantages but also some shortcomings. Perhaps the most obvious limitation concerns the use of the vector auto-regressive model which is viewed by some to be a simplified characterization of the highly complex spatio-temporal brain hemodynamic response. Despite its apparent simplicity, the VAR model is quite rich in capturing a broad range of temporal dynamics made possible by adjusting the maximal lag (or model order). Moreover, its simplicity provides considerable flexibility thereby allowing tests for effects of factors (e.g., experimental conditions, patient groups) and effects of covariates (e.g., age, gender and measurements of behavioral performance) on brain effective connectivity. In this paper, we apply the proposed ME-VAR model to investigate brain effective connectivity in neocortical areas involved in decision-making and action selection cognitive task. The fMRI data were collected while healthy young adults reached toward self-selected visible targets or toward specified visually cued targets.

The remainder of this paper is organized as follows. In the second and third sections, we develop the mixed effects vector autoregressive model. In the fourth section, we analyze the fMRI dataset to determine connectivity in the frontal, parietal and pre-motor regions. Concluding remarks are given in the fifth section.

The mixed effects VAR model

Consider a brain network with R regions of interest (ROIs), in this work we assume that each ROI has only one representative fMRI time series. In our mixed effects vector auto-regressive model (ME-VAR), we shall focus only on the pre-selected ROIs. Let $Y_r^s(t)$ the fMRI time series at the r-th ROI for participant s and denote the collection of observations at time t at all ROIs to be $\mathbf{Y}^s(t) = [Y_1^s(t),\ldots, Y_R^s(t)]'$. We shall assume that the fMRI data has undergone the standard pre-processing steps including slice timing correction, motion correction, removal of physiological signal of non-interest (cardiac and respiratory), co-registration, mild spatial smoothing and normalization to a common space.

To capture cross-dependence and lead-lag structure between all the pre-selected ROIs in a network, we start by specifying the general additive model,

$$\mathbf{Y}^s(t) = \mathbf{F}^s(t) + \mathbf{E}^s(t), t = 1,\ldots, T, \tag{1}$$

where

(a.) $\mathbb{E}\mathbf{Y}^s(t) = \mathbf{F}^s(t)$ (dimension $R\times 1$) is the participant-specific expectation that models the condition-specific deterministic trends in $\mathbf{Y}^s(t)$.

(b.) $\mathbf{E}^s(t)$ is a stochastic process, with $\mathbb{E}\mathbf{E}^s(t) = 0$ and $\mathbb{C}\mathrm{ov}[\mathbf{E}^s(t+h), \mathbf{E}^s(t)] = \Sigma(h)$, that models the cross-dependence structure between-ROIs for participant s.

The mean component, $\mathbf{F}^s(t)$, includes systematic changes in the BOLD signal that may be attributed to the experimental conditions. The mean component is well studied and statistical inference is already developed (e.g., Worsley and Friston, 1995; Friston et al., 1995; Nichols and Holmes, 2002) and implemented in standard neuroimaging software such as Statistical Parametric Mapping (SPM), FMRIB Statistical Laboratory (FSL) and Analysis of Functional NeuroImages (AFNI).

The standard approaches decompose the participant-specific mean component $\mathbf{F}^s(t)$ into

$$\mathbf{F}^s(t) = \beta_1^s \otimes X_1(t) + \ldots + \beta_C^s \otimes X_C(t),$$

where $\otimes$ denotes the Kronecker product; C is the number of experimental conditions; $X_c(t)$ (dimension 1×1) is the expected BOLD response associated with stimulus type c so that $X_c(t)$ is the convolution between the hemodynamic response function and the block design function for condition $c = 1,\ldots, C$. The participant-specific parameter vector for condition c is $\beta_c^s = [\beta_{c1}^s,\ldots, \beta_{cR}^s]'$ (dimension $R\times 1$) which indicates the amplitude of activation due to condition c at all the ROIs.

Our prime attention is devoted to developing brain connectivity models that we implement by specifying the covariance structure for the stochastic component $\mathbf{E}^s(t)$. We will see first that, under the assumption of weak temporal stationarity, the connectivity between ROIs is directly captured by the covariance structure of the stochastic component $\mathbf{E}^s(t)$,

$$\begin{aligned}\mathbb{C}\mathrm{ov}\left[\mathbf{Y}^s(t+h), \mathbf{Y}^s(t)\right] &= \mathbb{C}\mathrm{ov}\left[\mathbf{F}^s(t+h) + \mathbf{E}^s(t+h), \mathbf{F}^s(t) + \mathbf{E}^s(t)\right] \\ &= \mathbb{C}\mathrm{ov}\left[\mathbf{E}^s(t+h), \mathbf{E}^s(t)\right].\end{aligned}$$

Thus, one models the cross-dependence between the ROIs via the stochastic term $\mathbf{E}^s(t)$. Since $\mathbf{E}^s(t)$ cannot be directly observed, we shall use the residuals that mimic $\mathbf{E}^s(t)$ in Eq. (1),

$$\mathbf{R}^s(t) = \mathbf{Y}^s(t) - \hat{\mathbf{F}}^s(t), \tag{2}$$

where $\hat{\mathbf{F}}^s(t)$ is the participant specific mean estimate from the model in Eq. (1).

The mixed effects model for the stochastic component $\mathbf{E}^s(t)$

We propose the following mixed effects vector autoregressive model (ME-VAR) to describe cross-dependence in the stochastic component $\mathbf{E}^s(t)$ (dimension $R\times 1$). The proposed model will be used to investigate inquiries such as (i.) time lag dependence between each pair of ROIs; (ii.) testing for Granger causality for each experimental condition (iii.) testing differences in connectivity across experimental conditions.

The formal definition of the ME-VAR model of order P for participant s in an experiment with 2 conditions is

$$\mathbf{E}^{(s)}(t)=\sum_{k=1}^{P}\left[\Phi_{1,k}^{(s)}W_1^{(s)}(t)+\Phi_{2,k}^{(s)}W_2^{(s)}(t)\right]\mathbf{E}^{(s)}(t-k)+\mathbf{e}^{(s)}(t) \tag{3}$$

where $t=P+1,\ldots, T$, are the time points $s=1,\ldots, S$ represents participants and the vector $\mathbf{e}^{(s)}(t)$ (dimension $R\times 1$) has $\mathbb{E}\mathbf{e}^{(s)}(t)=0$ and $\mathbb{C}\mathrm{ove}^{(s)}(t)=\Gamma$. To describe the model, we first enumerate its basic elements.

1 *The maximal lag or order P*. The optimal order can be objectively selected using information theoretic criteria, that balances fit and complexity (where model complexity is measured as a function of the number of unknown parameters). In our implementation we used BIC (Bayesian information criterion) which is known to impose heavier penalty for complexity than AIC (Akaike information criterion) and thus tends to produce less complex models (e.g., models with lower order).
In theory, the ME-VAR model may allow subject-specific order but the computational complexity resulting from such generalization far outweighs practical benefits. Thus, in practice, we recommend that subjects share the same model order P. This model order is selected from the BIC corresponding to the VAR mixed effects model, then the order selection integrates the information from all the subjects to choose the optimal order.
2 *The participant-specific direct connectivity matrix at lag k, denoted* $\Phi_{c,k}^{(s)}$. This $R\times R$ matrix quantifies exactly how $\mathbf{E}^s(t-k)$ directly predicts $\mathbf{E}^s(t)$, under experimental condition c. We qualify the word "directly" because for VAR models, $\mathbf{E}^s(t-k)$ may *indirectly* predict $\mathbf{E}^s(t)$ via the intervening observations $\mathbf{E}^s(t-k+1)$ through $\mathbf{E}^s(t-1)$. There will be a specific direct connectivity matrix for each experimental condition and each time lag. In Eq. (3), the direct connectivity matrix includes a participant-specific random effect to describe the variability in the connectivity pattern across different participants.
3 *The participant-specific indicator function for condition c, denoted* $W_c^{(s)}(t)$. This function is used as a tool to differentiate brain connectivity across conditions. Suppose that at time t_0 a stimulus for condition c was presented; followed by a different condition c' at the time t_1. We specify the function $W_c^{(s)}(t)$ as a time window on which the brain connectivity present is attributed to condition c in participant s. This time window takes a value of 1 in the interval $[t_0, t_1]$ and takes the value 0 elsewhere. One may use a more general window that has a gradual rise from 0 to 1 in the time interval t_0 to $(t_0+\tau_0)$ and then a gradual decrease from 1 back to 0 on the time interval t_1 to $(t_1+\tau_1)$. The values for τ_0 and τ_1 could vary across conditions and participants and deserves to be carefully studied in fMRI experiments.

An example: ME-VAR model of order 1

To illustrate the features of the model, suppose that lag order is $P=1$ so that conditional mean of the observed BOLD signal at time t depends only on the observations at the previous time point $t-1$. The model for participant s is specified as

$$\mathbf{E}^{(s)}(t)=\left[\Phi_{1,1}^{(s)}W_1^{(s)}(t)+\Phi_{2,1}^{(s)}W_2^{(s)}(t)\right]\mathbf{E}^{(s)}(t-1)+\mathbf{e}^{(s)}(t) \tag{4}$$

where $\mathbf{e}^{(s)}(t)$ is a zero-mean white noise process with covariance matrix $\mathbb{C}\mathrm{ove}^{(s)}(t)=\Gamma$ that does not change over time and it is assumed to be constant across all participants.

Condition-specific effective connectivity

The first key elements for the participant-specific model in Eq. (4) are the connectivity parameter matrices $\Phi_{1,}^{(s)}{}_1$ and $\Phi_{2,}^{(s)}{}_1$ (dimension $R\times R$), which model subject condition-specific effective connectivity at lag 1.When condition 1 is "active" at time t then $W_1^{(s)}(t)=1$. Consequently, the effective connectivity for participant s at time lag t is $\Phi_{1,1}{}^{(s)}$. Vice versa, when condition 2 is "active" at time t, then $W_2^{(s)}(t)=1$ and, consequently, effective connectivity at time t is $\Phi_{2,}^{(s)}{}_1$. In particular, the effective connectivity model for the r-th ROI when condition 1 is active is written as

$$E_r^{(s)}(t)=\Phi_{1,1}^{(s)}(r,1)E_1^{(s)}(t-1)+\ldots+\Phi_{1,1}^{(s)}(r,R)E_R^{(s)}(t-1)+e_r^{(s)}(t),$$

and when condition (2) is active, it is written as

$$E_r^{(s)}(t)=\Phi_{2,1}^{(s)}(r,1)E_1^{(s)}(t-1)+\ldots+\Phi_{2,1}^{(s)}(r,R)E_R^{(s)}(t-1)+e_r^{(s)}(t).$$

Testing for significance of effective connectivity

When we reject the null hypothesis that $\Phi_{c,\,1}(r,r')=0$, we conclude that at population level the current hemodynamic activity at ROI r during condition c is significantly explained by the past hemodynamic activity at ROI r'. In this case, we can say that the hemodynamic activity at ROI r' "Granger-causes" the activity at ROI r. For a model of order P, this null hypothesis is expressed as $\Phi_{c,\,1}(r,r')=\Phi_{c,\,2}(r,r')=\ldots=\Phi_{c,\,P}(r,r')=0$.

Testing for differences across experimental conditions

One of our primary goals is to investigate differences in brain connectivity between experimental conditions. Under the proposed model, this is equivalent to comparing the components of matrices $\Phi_{1,\,k}$ and $\Phi_{2,\,k}$ for each time lag $k=1,\ldots, P$. This test is conducted using the equivalent representation of the ME-VAR model of Eq. (3),

$$\mathbf{E}^{(s)}(t)=\sum_{k=1}^{P}\left[\Phi_{1,k}+\Delta_k W_2^{(s)}(t)+\mathbf{b}_k^{(s)}\right]\mathbf{E}^{(s)}(t-k)+\mathbf{e}^{(s)}(t), \tag{5}$$

by testing directly the parameter matrix Δ_k (dimension $R\times R$) via $H_0:\Delta_k=0$ for $k=1,\ldots, P$. Note that when $\Delta_k\neq 0$ then the effective connectivity for the two conditions is different at lag k.

Using a similar formulation, one can also test for differences in effective connectivity across disease groups and interactions between experimental conditions and disease groups.

Modeling variation in effective connectivity across participants

The second key element in Eq. (4) is the superscript *(s)* in the connectivity parameter matrices that indicates that brain connectivity is allowed to vary over participants. Here, we decompose the connectivity matrix into fixed and random components

$$\Phi_{c,k}^{(s)}=\Phi_{c,k}+\mathbf{b}_k^{(s)}, \tag{6}$$

where $\Phi_{c,\,k}$ (dimension $R\times R$) is the condition-specific (fixed effect) connectivity matrix common in a population from which the subjects were sampled and $\mathbf{b}_k^{(s)}$ (dimension $R\times R$) is the participant-specific (random effect) which models an individual participant's deviation from the common population-specific connectivity matrix associated

to lag k. Here, we model the elements of the matrix $\mathbf{b}_k^{(s)}$ as mutually independent Gaussian random variables

$$b_k^{(s)}(i,j) \sim N\left(0, \sigma_k^2(i,j)\right).$$

Some remarks on the model

In the next mathematical derivations, we shall establish the following: (1.) the ME-VAR model admits contemporaneous cross-correlation (zero order connectivity) between ROIs; (2.) the connectivity structure, as modeled by the covariance matrix of $\mathbf{E}^{(s)}(t)$, is allowed to vary across participants even if we adopt the simplifying assumption that $\mathbb{C}\mathrm{ov}\mathbf{e}^{(s)}(t) = \Gamma$ is constant across participants.

Under the ME-VAR model, subject specific zero order connectivity (instantaneous correlation between ROIs) is completely determined by the lagged matrices $\Phi_1^{(s)}{}_1$, $\Phi_2^{(s)}{}_1$ and the noise covariance Γ. To see this, denote $\mathbf{M}_s = \left[\Phi_{1,k}^{(s)} W_1^{(s)}(t) + \Phi_{2,k}^{(s)} W_2^{(s)}(t)\right]$. It then follows that

$$\mathbf{E}^{(s)}(t) = \mathbf{M}_s \mathbf{E}^{(s)}(t-1) + \mathbf{e}^{(s)}(t)$$

where, $\mathbb{E}\left(\mathbf{e}^{(s)}(t)\right) = 0$, $\mathbb{C}\mathrm{ov}\left(\mathbf{e}^{(s)}(t), \mathbf{e}^{(s)}(t)\right) = \Gamma$, and $\mathbb{C}\mathrm{ov}\left(\mathbf{e}^{(s)}(t), \mathbf{e}^{(s)}(k)\right) = 0$. Then, the subject-specific covariance matrix at zero lag is given by

$$\mathbb{C}\mathrm{ov}\left(\mathbf{E}^{(s)}(t)\right) = \sum_{i=0}^{\infty} \mathbf{M}_s^i \Gamma \mathbf{M}_s^{i'} \tag{7}$$

where the matrices $\mathbf{M}_s^i$ represent subject specific coefficient matrices to the i-th power which are absolutely summable under the vector autoregressive framework (Lutkepohl, 1993). Clearly, Eq. (7) demonstrates (1.) and (2.) above.

It is also possible to consider a subject specific noise covariance $\Gamma^{(s)}$ or to have group-specific noise covariance. However, these are not necessary as the group or covariate effect on connectivity as well as the variation in connectivity across participants are already captured by $\mathbf{M}_s$. Moreover, for computational simplicity, we shall constrain Γ to be a diagonal matrix. This simplifying assumption does not lead to a zero cross-covariance (See Eq. (7)). This constraint allows fitting the model marginally and avoids the computational problems that arise when the model is fitted jointly and the length of time series, number of multivariate entries and random effects is large (Schafer and Yucel, 2002). In fact, tests of hypothesis on Granger causality and parameter significance are constructed marginally and thus justify our approach of marginal fitting.

Note that a more complex model will not assume independence between the elements of the random effects matrix. Thus

$$\mathbb{C}\mathrm{ov}\left(\Phi_{c,k}^{(s)}(i,j), \Phi_{c,k}^{(s)}(n,m)\right) = \mathbb{C}\mathrm{ov}\left(b_k^{(s)}(i,j), b_k^{(s)}(n,m)\right)$$

could be different from zero. Consequently we would allow high values of connectivity, expressed by $\Phi_{c,k}^{(s)}(i,j)$, to be associated with high or low values in $\Phi_{c,k}^{(s)}(n,m)$. It will be of interest to study the impact on model fitting when we relax this assumption.

As a final remark, Eq. (6) suggests that, due to the natural variability between subjects, it is possible for some individuals to have high connectivity values even when the group average is low. Thus, it is important to identify pairs of ROIs whose inter-regional connectivity are stable (have low variation) in the patient group as well as those pairs of ROIs that exhibit large variation as this information could be useful for understanding differences between patient groups.

Estimation of the connectivity parameters in the ME-VAR model

To estimate the connectivity parameters, we shall use the conditional maximum likelihood procedure as described in Shumway and Stoffer (2006). When the model order is $P=1$, we treat the first observation $\mathbf{E}(1)$ as fixed, then conditional likelihood for participant s is

$$f\left(\mathbf{E}^{(s)}(2),\ldots,\mathbf{E}^{(s)}(T)\middle|\mathbf{E}^{(s)}(1),\mathbf{b}_1^{(s)}\right) = f\left(\mathbf{E}^{(s)}(2)\middle|\mathbf{E}^{(s)}(1),\mathbf{b}_1^{(s)}\right)\times\ldots \times f\left(\mathbf{E}^{(s)}(T)\middle|\mathbf{E}^{(s)}(1),\ldots,\mathbf{E}^{(s)}(T-1),\mathbf{b}_1^{(s)}\right).$$

The formulation above yields substantial simplification in computation because under the ME-VAR model with P = 1, for example, the conditional distribution of $E^{(s)}(t)$ is Gaussian with mean and variance, respectively,

$$\left[\Phi_{1,1}^{(s)} W_1^{(s)}(t) + \Phi_{2,1}^{(s)} W_2^{(s)}(t)\right]\mathbf{E}^{(s)}(t-1) \text{and} \Gamma.$$

This enables us to embed the estimation problem under the mixed models framework (Davidian, 2005; Diggle et al., 2002) and thus allows for the use of existing statistical software such as Statistical Analysis System (SAS) and R for model fitting. The fixed connectivity matrices $\Phi_{1,1}$ and $\Phi_{2,1}$ and the variance parameters Γ and $\sigma_1^2(i,j)$ are estimated in these software packages by conditional restricted maximum likelihood or conditional likelihood (SAS/STAT 9.2). Participant specific effects $\mathbf{b}_1^{(s)}$ are predicted using the empirical Bayes procedure.

Time lag dependence between each pair of brain regions is determined by testing the significance of each element of the connectivity parameter matrices $\Phi_{c,k}$ for each condition, using the Wald's test statistic. Evaluation of Granger causality is conducted by testing whether the past hemodynamic activity at ROI r' significantly improves prediction at ROI r. In this case we say that region r' "Granger causes" activity at region r for condition c if we reject the null hypothesis $\Phi_{c,1}(r,r') =, \ldots, = \Phi_{c,P}(r,r') = 0$, that is, if we declare that at least one of these connectivity parameters is statistically different from zero.

Under the model in Eq. (3), there are $R*R*P*2$ parameters in the coefficient matrices, where R is the number of ROIs, P is the model order and 2 stands for the number of conditions. Additionally we perform $R*R*2$ tests corresponding to Granger causality. It is necessary to correct for multiple comparisons. In our analysis, we applied the false discovery rate procedure (FDR) at level 0.05.

Connectivity analysis of the fMRI data

To investigate brain connectivity implicated in decision-making, we used the ME-VAR model to fMRI data collected from 15 participants while they were performing a visual-motor task.

Data description

Participants

We recruited 15 healthy participants from the Brown University community having a mean age of 26.5 ?± 5.4 year; 4 females; all right-handed (as assessed by a modified handedness scale, Olfield, 1971). No participant had a history of neurological or motor/sensory disorder.

Tasks, apparatus and procedures

Participants performed a center-out goal-directed wrist movement using an MRI-compatible joystick (Mag Design and Engineering, Sunnyvale, CA) with their right hand.

Visual stimuli, which appeared on a projection screen, consisted of a "home" position (a black round dot of diameter 4 cm) always visible located in the center of the visual display; targets (black round dots of diameter 3 cm) that could appear at 12different locations (30° apart) around a circle at 5 cm from the "home" position and a green or red dot (1 cm diameter) which appeared at one of the 12 locations around a circle at 1.5 cm from the "home" position. Joystick movement displaced a cursor (a black round dot of diameter 0.75 cm) over a white background.

We designed an event-related fMRI experiment with jittered trials duration (10, 11, 12, or 13 s). The experiment comprised two main conditions, a "Free" condition and an "Instructed" condition. For each condition, a trial began with the appearance of the central "home" position target (500 ms) followed by the presentation of four of the 12 targets and of the green dot. To select which of the 12 targets would appear, we divided the visual display into four quadrants containing three targets each and randomly choose one target per quadrant. Participants could initiate reaching movements as soon as the targets appeared. They repositioned the cursor in the "home" position after each reach.

In the Free choice condition, participants reached to one of the four targets of their own choice; participants were told before each MRI session that the green dot location was meaningless. In the Instructed condition, the green dot was always aligned with one of the four targets and participants had to reach to that target. Thus, in the Free condition, participants had to decide which of the four targets they would move toward, whereas in the Instructed condition, they had to move toward the target specified by the green dot.

We presented different sets of four targets on each trial, as opposed to have the same four targets at the same location, to limit or even prevent participants from deciding in advance which target they would visit and also to reduce the possibility that they would implement a conscious or unconscious strategy for selecting which target to visit from trial to trial.

The experiment was divided in 10 consecutive fMRI runs, alternating between the two conditions but always starting with the Free condition. In each fMRI run, participants performed 20 trials (when the dot was green) and 5 null trials (when the dot was red) for a total of 100 movement trials for each of the Free and Instruction conditions. In the null trials, one per block of 5 trials, participants were instructed not to move. A short break of less than 1 min separated each MRI run.

MR imaging

We used a 3T Tim Trio MRI system (Siemens Medical Solutions, Erlangen, Germany) to acquire anatomical and functional fMRI images. The magnetic field was shimmed before to MR data acquisition. For the fMRI data, we generated T2 -weighted gradient echo images (EPI) using the blood oxygenation level-dependent (BOLD) mechanism (Bandettini et al., 1992; Kwong et al., 1992) with the following parameters: TR = 1 s, TE = 28 ms, field of view = 192 mm, image matrix = ?64×64, flip angle of 90°, 3 mm slice thickness, and 20 slices per volume cover the uppermost portions of parietal and frontal cortices. We also acquired a high resolution three-dimensional anatomical image consisting in 160 1-mm sagittal slices (magnetization prepared rapid acquisition gradient echo sequence, MPRAGE, with TR = 1900 ms, TE = 2.98 ms, 1 mm isotropic voxels, 256 mm field of view). The MRI system acquired the functional MR images in an interleaved manner and did not collect any data for the first seven EPI volumes of each run because of T1 saturation effect. We acquired 300 EPI volumes for each of 10 MRI runs.

Selection of regions of interest

The fMRI data were preprocessed and areas of activation were selected from the results of a general linear model. We used AFNI (Analysis of Functional NeuroImages; Medical College of Wisconsin; National Institute of Health: http://afni.nimh.nih.gov/afni, Cox and Hyde, 1997; Cox, 1996) and FSL software packages (FMRIB software Library, http://www.fmriib.ox.ac.uk/fsl/, Smith et al., 2004) to process, analyze and visualize MRI images. We first scaled each of the EPI time series by their mean and multiplied by 100 to yield a percentage signal change. We then concatenated these time series and used a six-parameter rigid-body cubic polynomial interpolation (3dvolreg tool in AFNI) to motion correct these referring to the third image acquired and adjusted for slice timing offset. Baseline drift was removed with quadratic polynomial during the regression procedures for each run separately (see below). We then co-registered and normalized the anatomical and functional data sets to the MNI152 template (FLIRT tool in FSL) and finally spatially smoothed the functional data set with a 6 mm full-width half-maximum Gaussian kernel.

Events of interest for the GLM analysis consisted of when the four targets appeared, these events were convolved with a gamma variate function (Cohen et al., 1997) to yield an impulse response function. We then used these reference functions and the six motion correction parameters (Johnstone et al., 2006) as inputs to a multiple regression analysis (3dDeconvolve tool in AFNI) to estimate the weights of each condition. We determined areas of differential activation across the two conditions by retaining voxels that were significantly different between the two conditions, that is with a p-value$_?$<0.001 and t-statistic$_?$<4.116, corrected for multiple comparisons at p-value = 0.05 for 10 contiguous voxels (alpshasim tool in AFNI). To localize activation to brain areas, we used the brain atlas of Duvernoy (1991) and a navigable web-based human brain atlas (https://msu.edu/~brains/brains/human/index.html). The ROIs and their corresponding MNI coordinates are reported in Table 1 and are displayed in Fig. 1. The activated regions included portions of the prefrontal cortex (PFC), premotor cortex, dorsal (PMd) and ventral (PMv) regions, the supplementary motor area (SMA), all infrontal cortex and a region located within the intraparietal sulcus (IPS) and a broad expanse of the superior parietal lobule (SPL). All these showed more activation for Free than Instructed. The participant-specific fMRI time series at these ROIs were then extracted for connectivity analysis.

Fitting the ME-VAR model for investigating effective connectivity

We computed the participant specific residuals $\mathbf{R}^s(t) = \mathbf{Y}^s(t) - \hat{\mathbf{F}}^s(t)$ in Eq. (2). The deterministic trend $\hat{\mathbf{F}}^s(t)$ was obtained as the estimated expectation of a linear model that comprises participant-specific estimated drift, motion correction, oscillations that correspond to the respiratory- and cardiac-related non-interest physiological signals and condition-specific changes in the mean level of activation. All these were derived from the previous activation analysis using AFNI.

The optimal order was determined by the Bayesian Information Criterion (BIC) to be $P = 2$ which roughly corresponds to a 2 second lag. The maximal order considered was $P_{\max} = 8$. which roughly corresponds to 8 s and thus is sufficiently large for most fMRI data analysis. The parameters in the ME-VAR model were estimated using the procedure proc mixed in the (Statistical Analysis System) SAS Institute Inc. (2008). Hypothesis testing procedures were also carried out in SAS software correcting for multiple comparisons by the false discovery rate (FDR) procedure at the rate of 0.05.

Discussion of results

To investigate lag cross-dependence structure in each condition , we tested the significance of each element in the connectivity matrices $\Phi_{c,k}$. The estimated elements of parameter matrices for condition Free and Instructed are showed in Table 2 for lag 1 and in Table 3 for lag 2. Elements in bold indicate coefficients significantly different from zero.

Table 1
Regions of interest and the MNI coordinates. MNI coordinates indicate voxel with the highest MRI signal values, with positive X coordinates indicating right hemisphere. BA, Brodmann areas. Volume represents the cluster volume in mm^3.

Brain regions	BA	Volume	MRI signal		MNI coordinates		
			Mean	Max	X	Y	Z
R superior partial lobule	7	14,175	0.12	0.18	2	59	48
R pre-motor dorsal	6	2916	0.10	0.18	−29	5	63
L pre-supplementary motor areas	8	1674	0.11	0.16	2	−14	45
L pre-motor dorsal	6	1404	0.10	0.14	29	8	66
R pre-motor ventral	6	1053	0.16	0.22	−44	−5	36
L pre-frontal cortex	46	702	0.12	0.16	35	−53	24
L intra-parietal sulcus	7	405	0.10	0.12	35	53	39

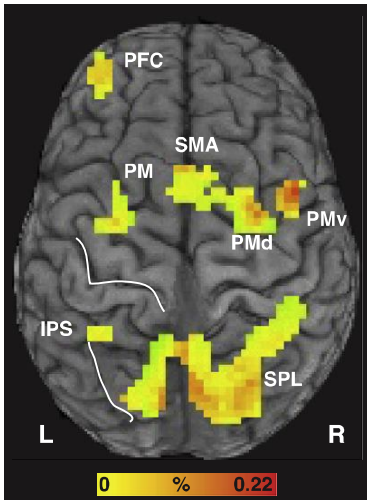

Fig. 1. Areas of differential task-related activation across the two conditions. Color code represents intensity of activation. White lines represent central sulcus and intra-parietal sulcus. For interpretation of the references to color in this figure legend, the reader is referred to the web version of this article.

If the component (r, r') in the connectivity matrix $\Phi_{c,k}$ is significantly different from zero, we may conclude that under condition c, current hemodynamic activity at ROI r depends on the past (lag k) hemodynamic activity at the r'-th ROI.

We implemented a Granger causality analysis using the mixed-effect VAR strategy as described above to identify effective connectivity in pairs of brain regions previously identified as exhibiting task-related activation; Fig. 2 illustrates statistically significant interactions between the activated areas for the Free (left) and Instructed (right) tasks. Each link in these graphs indicates that activity in one of the ROIs Granger causes activity in other ROIs, meaning that if at least one connection from first region to the second over all time lags is statistically non zero then we have a link.

Table 2
Connectivity matrices estimates at lag 1. Elements in bold indicate coefficient is significantly different from zero at level 0.05 with FDR correction.

	PFC	R PMv	R SPL	IPS	R PMd	SMA	L PMd
Effect of condition Free at lag 1 ($\Phi_{1,1}$)							
PFC	**0.600**	0.034	0.015	**0.074**	0.012	0.030	0.049
R PMv	0.030	**0.318**	**0.050**	**0.037**	**0.069**	**0.059**	**0.089**
R SPL	0.013	**0.078**	**0.223**	**0.094**	**0.069**	0.006	**0.080**
IPS	**0.042**	**0.086**	**0.058**	**0.318**	**0.046**	0.013	**0.082**
R PMd	**0.041**	**0.090**	**0.039**	**0.034**	**0.314**	0.025	**0.097**
SMA	**0.071**	**0.091**	0.018	**0.033**	0.035	**0.391**	**0.111**
L PMd	**0.050**	**0.076**	0.017	**0.052**	**0.065**	**0.041**	**0.370**
Effect of condition Instructed at lag 1 ($\Phi_{2,1}$)							
PFC	**0.621**	0.023	0.004	**0.071**	0.013	**0.036**	0.028
R PMv	0.012	**0.313**	**0.049**	**0.047**	**0.074**	**0.045**	**0.093**
R SPL	0.004	**0.076**	**0.277**	**0.067**	**0.071**	0.014	**0.065**
IPS	**0.033**	**0.076**	**0.069**	**0.325**	**0.041**	0.014	**0.096**
R PMd	0.023	**0.080**	**0.057**	**0.038**	**0.310**	0.018	**0.076**
SMA	**0.063**	**0.089**	**0.030**	**0.036**	0.033	**0.391**	**0.088**
L PMd	**0.020**	**0.068**	0.020	**0.036**	**0.046**	**0.028**	**0.386**
Difference Instructed-Free at lag 1							
PFC	0.021	−0.012	−0.010	−0.003	0.001	0.007	−0.021
R PMv	−0.018	−0.005	−0.001	0.010	0.005	−0.014	0.005
R SPL	−0.009	−0.002	0.054	**−0.027**	0.002	0.008	−0.014
IPS	−0.010	−0.010	0.011	0.008	−0.005	0.001	0.014
R PMd	−0.017	−0.010	0.017	0.004	−0.003	−0.006	−0.021
SMA	−0.008	−0.002	0.013	0.002	−0.002	0.000	−0.023
L PMd	**−0.030**	−0.007	0.003	−0.016	−0.019	−0.012	0.016

Table 3
Connectivity matrices estimates at lag 2. Elements in bold indicate coefficient is significantly different from zero at level 0.05 with FDR correction.

	PFC	R PMv	R SPL	IPS	R PMd	SMA	L PMd
Effect of condition Free at lag 2 ($\Phi_{1,2}$)							
PFC	**0.204**	−0.013	**−0.042**	−0.010	−0.016	−0.005	−0.022
R PMv	**−0.026**	**0.103**	−0.009	−0.021	−0.021	−0.003	−0.021
R SPL	−0.025	**0.042**	**0.131**	0.008	−0.011	−0.001	0.019
L SPL	−0.025	0.005	0.018	**0.124**	−0.011	−0.001	0.030
R PMd	**−0.036**	0.024	−0.012	−0.016	**0.128**	−0.003	−0.004
SMA	**−0.036**	**0.027**	−0.029	−0.029	−0.022	**0.173**	−0.017
L PMd	**−0.027**	0.021	−0.007	**−0.028**	−0.017	−0.017	**0.094**
Effect of condition Instructed at lag 2 ($\Phi_{2,2}$)							
PFC	**0.182**	−0.010	−0.017	−0.022	−0.012	−0.023	−0.021
R PMv	−0.017	**0.120**	−0.010	**−0.023**	0.000	−0.001	−0.032
R SPL	−0.018	0.014	**0.133**	0.012	0.014	−0.013	0.000
L SPL	−0.017	0.003	0.009	**0.153**	−0.002	−0.016	0.018
R PMd	**−0.021**	0.019	0.002	−0.008	**0.137**	0.003	0.003
SMA	**−0.041**	**0.026**	−0.005	**−0.032**	−0.014	**0.169**	−0.023
L PMd	**−0.016**	0.016	−0.011	**−0.018**	0.006	−0.015	**0.112**
Difference Instructed-Free at lag 2							
PFC	−0.022	0.003	0.025	−0.012	0.004	−0.018	0.001
R PMv	0.009	0.017	−0.001	−0.002	0.021	0.002	−0.010
R SPL	0.007	**−0.028**	0.002	0.004	0.025	−0.012	−0.019
IPS	0.008	−0.002	−0.008	0.029	0.009	−0.015	−0.012
R PMd	0.015	−0.005	0.014	0.008	0.009	0.006	0.007
SMA	−0.005	0.000	0.024	−0.003	0.008	−0.004	−0.006
L PMd	0.011	−0.005	−0.003	0.010	0.023	0.002	0.018

The analysis revealed both statistically significant unidirectional (yellow lines) and bidirectional (blue lines) effective connectivity between areas. For both tasks, note that most regions had bidirectional connectivity, both within and between frontal and parietal cortices. Unidirectional connectivity from frontal areas tended to influence other frontal regions, with the exception of a significant influence from the left PMd to the contralateral SPL. IPS and SPL had mutual connections and unidirectional feed-forward connections to frontal regions, specifically SMA (both tasks) and PFC (Free task only).

We next directly contrasted connectivity patterns obtained during the Free and the Instructed task (Fig. 3), evaluated at lag 1 (Fig. 3A) and lag 2 (Fig. 3B). For this analysis, we found enhanced connectivity during the Free compared to the Instructed task from the left PFC to the left PMd and also from the left IPS to the right SPL at lag 1 (Fig. 3A). At lag 2, the connection from the right PMv to the right SPL was stronger during the Free compared to the Instructed task. Details of the estimates for the effective connectivity patterns comparing the Free and Instructed tasks appear in Table 2 for lag 1 and in Table 3 for lag 2.

Region PFC is involved in higher cognitive control such as decision making and action selection (Barraclough et al., 2004; Miller and Cohen, 2001). PFC lesions often impair planning, decision making, and executive control (Wilson et al., 2010). Region PMd also is involved in movement planning and execution and it can encode multiple potential reaches (Cisek and Kalaska, 2005). Thus, the higher connectivity from PFC towards PMd, in the Free condition, could relate to a selection mechanism by PFC of one of the motor plans elaborated in PMd.

We also found stronger connectivity from left IPS towards right SPL in the Free condition than in the Instructed. The parietal lobe is well known to be involved in visuo-motor actions such as goal-directed reaching movements (Andersen and Cui, 2009; Karnath and Perenin, 2005) but also in decision making (Glimcher, 2003). Therefore increased connectivity in the Free condition between parietal regions of each hemisphere could relate to greater demands of visuo-spatial processing of all potential targets.

Although the main interest relies in the estimation and inference of connectivity matrices, in the context of mixed effects model it is also useful to consider estimation of the random effects variability. This

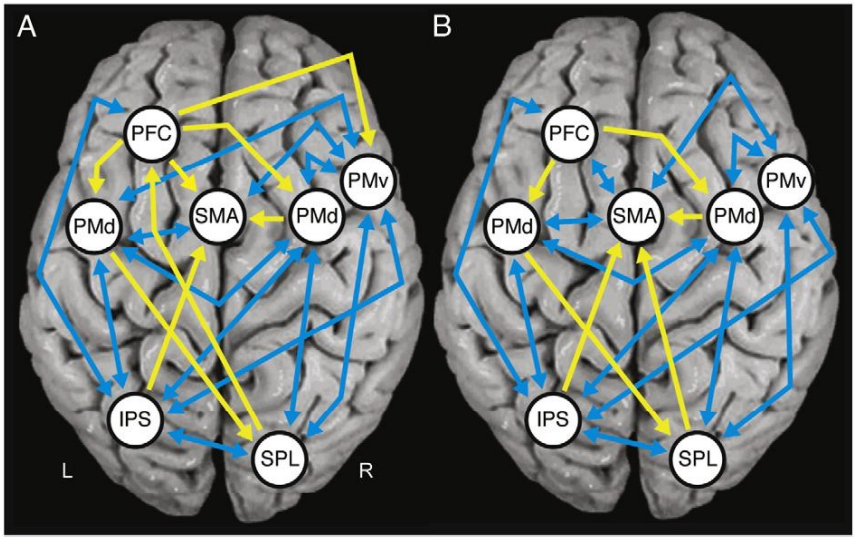

Fig. 2. Granger causality interactions between ROIs. Links between two ROIs represent that past hemodynamic activity in one region helps to predict current hemodynamic activity in the other region. Yellow arrows indicate unidirectional associations and blue arrows bidirectional associations. A. Free condition. B. Instructed condition. For interpretation of the references to color in this figure legend, the reader is referred to the web version of this article.

variability indicates the general deviation of the participants from the mean connectivity parameters at each lag time, providing information about the robustness across participants in the parameters of interest. Table 4 shows the variability for both conditions in brain connectivity matrices for the 15 participants in the experiment at each lag. Strength of variability is displayed in Fig. 4A. Major variability at lag 1 is localized in the diagonal elements of the table, indicating that the dominant source of variation between participants refers to how previous activity in brain regions affects themselves at the current time. Also there is an important variation across participants in how region PFC is affected by the others and in the way that left PMd and right PMV influences most of the regions (Fig. 4B).

Conclusions and further discussion

In this paper we proposed to study brain connectivity patterns using the ME-VAR model. Our model is a generalization of the usual VAR model because it incorporates random effects to depict the natural variability in connectivity between participants. It is important to account for variation in the connectivity patterns in order to produce a more accurate statistical inference on testing for Granger-causality and group comparisons. Moreover, the ME-VAR model has the flexibility to include covariate and group-specific parameters in the connectivity structure. This may be useful in situations where one would like to identify the pairs of ROIs that differentiate the healthy from the disease populations. Although the ME-VAR model requires complex statistical procedures for parameter estimation and inference, one may build on the existing statistical theory and utilize statistical software for general mixed effects models. Here, we implemented the model using the proc mixed procedure in the Statistical Analysis Software (SAS).

For further refinements of the ME-VAR model, it will be necessary to include spatial and between-subject variation in the HRFs. In the current model *fitting*, we assumed mutual independence on the random effect terms. It will be interesting to study the impact on model fitting

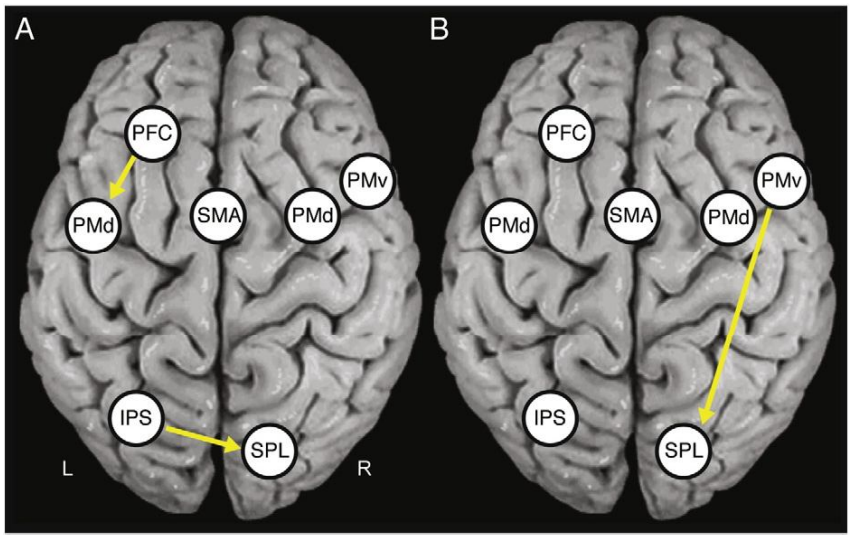

Fig. 3. Differences in connectivity between conditions for each lag. Arrows indicate the links at which there is a significant difference between conditions Free and Instructed. A. at lag 1. B. at lag 2.

Table 4
Standard deviation of random effects at Lag 1 and at Lag 2.

	PFC	R PMv	R SPL	IPS	R PMd	SMA	L PMd
Lag 1							
PFC	0.106	0.057	0.027	0.047	0.072	0.054	0.082
R PMV	0.033	0.098	0.055	0.039	0.040	0.044	0.040
R SPL	0.043	0.058	0.092	0.046	0.046	0.018	0.039
IPS	0.046	0.029	0.032	0.072	0.031	0.031	0.075
R PMd	0.035	0.048	0.028	0.028	0.136	0.040	0.077
SMA	0.037	0.063	0.034	0.029	0.046	0.095	0.055
L PMd	0.025	0.047	0.026	0.040	0.037	0.041	0.110
Lag 2							
PFC	0.065	0.013	0.033	0.035	0.058	0.062	0.036
R PMv	0.023	0.038	0.029	0.018	0.037	0.024	0.043
R SPL	0.030	0.023	0.031	0.037	0.028	0.036	0.032
IPS	0.030	0.029	0.019	0.045	0.025	0.025	0.038
R PMd	0.019	0.026	0.028	0.030	0.040	0.017	0.028
SMA	0.030	0.014	0.037	0.021	0.020	0.021	0.031
L PMd	0.014	0.026	0.029	0.012	0.036	0.026	0.051

when we relax this assumption. In addition, the ME-VAR model characterizes only linear associations. More general model should consider the inclusion of higher order and different interactions terms. There will be an explosion of the number of parameters but it is possible to build on existing theory for complexity-penalized regression.

We end this paper with a note that one has to exercise caution when interpreting results from any connectivity analysis using fMRI. As stated, fMRI measures brain hemodynamic activity and represents a proxy for the unobserved neuronal activity. Thus, connectivity interpretations from results derived in our model directly refer to the hemodynamic response. Using only the fMRI data at hand in the analysis it would not be possible to make inferences on the neuronal level without invoking models that explain the neuronal basis of the BOLD response—which is beyond the scope of this paper. Under the ME-VAR model, when a connectivity parameter is significant, then one may conclude that knowing the past BOLD response at ROI *A* gives a better prediction for the BOLD response at ROI *B*. The ME-VAR model explains the temporal sequence of dynamics in the BOLD response and thus, under the

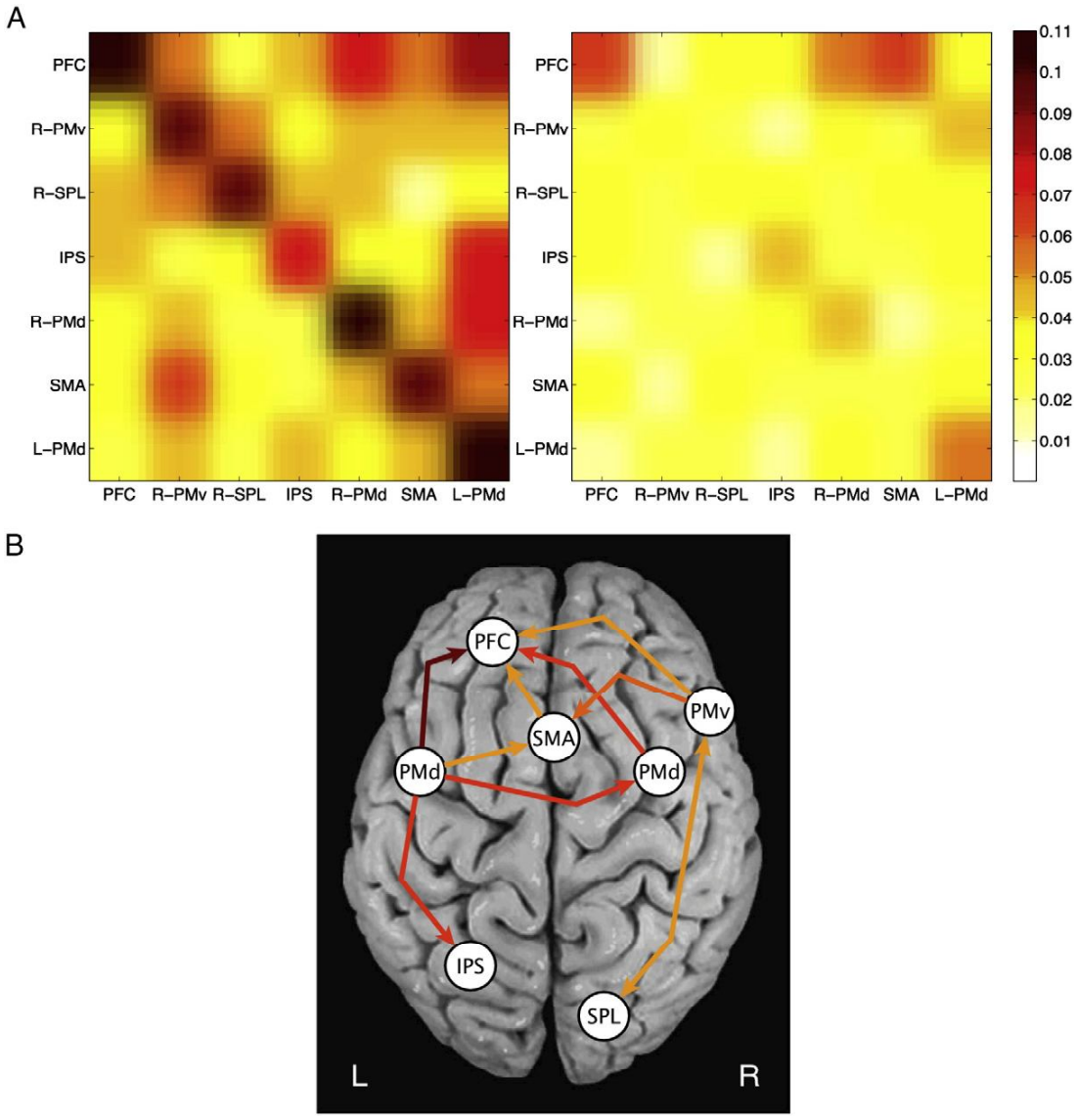

Fig. 4. Illustration of standard deviation of random effects $\mathbf{b}_k^{(s)}$. A. Standard deviation of random effects at Lag 1 (left) and at Lag 2 (right). B. Links with the strongest variation between participants at Lag 1.

framework of Granger causality, one can say that the BOLD response in ROI *A* "causes" the BOLD response in ROI *B*. Moreover, the current implementation of the ME-VAR model assumes that the underlying hemodynamic response function (HRF) is common across all ROIs. Thus, any statistically significant connectivity may be due to the different delays in the HRFs which might not be reflective of the actual temporal sequence of neuronal activity. Additionally, we have assumed that the HRFs are common across all subjects. The robustness of current model to violations of the common HRF assumption has not been investigated.

Acknowledgments

This research was supported in part by grants from the NSFDMS 0806106 (Ombao) and NSFBCS 0843938 (Sanes) and the CONACyT fellowship award from Mexico (Gorrostieta).

Appendix A. Supplementary data

Supplementary data to this article can be found online at doi:10.1016/j.neuroimage.2011.08.115.

References

Albouy, G., Sterpenich, V., Balteau, E., Vandewalle, G., Desseilles, M., Dang Vu, T., Darsaud, A., Ruby, P., Luppi, P., Degueldre, C., Peigneux, P., Luxen, A., Maquet, P., 2008. Both the hippocampus and striatum are involved in consolidation of motor sequence memory. Neuron 58, 261–272.

Andersen, A.R., Cui, H., 2009. Intention, action planning, and decision making in parietal–frontal circuits. Neuron 63, 568–583.

Assaf, M., Jagannathan, K., Calhoun, V.D., Miller, L., Stevens, M.C., Sahl, R., O'boyle, J.C., Schultz, R.T., Pearlson, G.D., 2010. Abnormal functional connectivity of default mode sub-networks in autism spectrum disorder patients. NeuroImage 53, 247–256.

Bandettini, A.P., Wong, C.E., Hinks, S.R., Tikofsky, S.R., Hyde, J.S., 1992. Time course EPI of human brain function during task activation. Magn. Reson. Med. 25, 390–397.

Barraclough, J.D., Conroy, L.M., Lee, D., 2004. Prefrontal cortex and decision making in a mixed-strategy game. Nat. Neurosci. 7, 404–410.

Benetti, S., Mechelli, A., Picchioni, M., Broome, M., Williams, S., Mcguire, P., 2009. Functional integration between the posterior hippocampus and prefrontal cortex is impaired in both first episode schizophrenia and the at risk mental state. Brain 132, 2426–2436.

Cadotte, A.J., Mareci, T.H., Demarse, T.B., Parekh, M.B., Rajagovindan, R., Ditto, W.L., Talathi, S.S., Dong-Uk, H., Carney, P.R., 2009. Temporal lobe epilepsy: anatomical and effective connectivity. IEEE Trans. Neural. Syst. Rehabil. Eng. 17, 214–223.

Chen, Y., Bressler, S.L., Ding, M., 2009. Dynamics on networks: assessing functional connectivity with Granger causality. Comput. Math. Organ Theory 15, 329170.

Cisek, P., Kalaska, F.J., 2005. Neural correlates of reaching decisions in forsal premotor cortex: specification of multiple direction choices and final selection of action. Neuron 45, 801–814.

Cohen, J.D., Perlstein, W.M., Braver, T.S., Nystrom, L.E., Noll, D.C., Jonides, J., Smith, E.E., 1997. Temporal dynamics of brain activation during a working memory task. Nature 386, 604–608.

Cox, R.W., 1996. AFNI: software for analysis and visualization of functional magnetic resonance neuroimages. Comput. Biomed. Res. 29, 162–173.

Cox, R.W., Hyde, J.S., 1997. Software tools for analysis and visualization of FMRI data. NMR Biomed. 10, 171–178.

Davidian, M., 2005. ST 732 Applied longitudinal data analysis. Lecture Notes. Department of Statistics North Carolina State University.

Diggle, P.J., Heagerty, P., Liang, K.Y., Zeger, L.S., 2002. Analysis of longitudinal data, Second edition. Oxford statistical science series, 25.

Duvernoy, H., 1991. The Human Brain. Surface, Three-Dimensional Sectional Anatomy and MRI. Springer-Verlag, New York.

Fiecas, M., Ombao, H., 2011. The generalized shrinkage estimator for spectral analysis of multivariate time series. Ann. Appl. Stat 5 (2A), 1102–1125.

Fiecas, M., Ombao, H., Linkletter, C., Thompson, W., Sanes, J., 2010. Functional connectivity: shrinkage estimation and randomization test. NeuroImage 40, 3005–3014.

Fleming, M.S., Thomas, L.C., Dolan, J.R., 2010. Overcoming status quo bias in the human brain. Proc. Natl. Acad. Sci. U.S.A. 107, 6005–6009.

Friston, K., Holmes, A., Worsley, K., Poline, J., Frith, C., Frackowiak, R., 1995. Statistical parametric maps in functional imaging: a general linear approach. Hum. Brain Mapp. 2, 189–210.

Glimcher, W.P., 2003. The Neurobiology of visual-saccadic decision making. Annu. Rev. Neurosci. 26, 133–179.

Goebel, R., Roebroeck, A., Kim, D., Formisano, E., 2003. Investigating directed cortical interactions in time-resolved fMRI data using vector autoregressive modeling and Granger causality mapping. Magn. Reson. Imaging 21, 1251–1261.

Harrison, L., Penny, W., Friston, K., 2003. Multivariate autoregressive modeling of fMRI time series. NeuroImage 19, 1477–1491.

Johnstone, T., Walsh, K.S.O., Greischar, L.L., Alexander, A.L., Fox, A.S., Davidson, R.J., Oakes, T.R., 2006. Motion correction and the use of motion covariates in multiple-subject fMRI analysis. Hum. Brain Mapp. 27, 77917.

Kaminski, M., Blinowska, K., 1991. A new method of the description of the information flow in the brain structures. Biol. Cybern. 65, 203–210.

Karnath, O.H., Perenin, T.M., 2005. Cortical control of visually guided reaching: evidence from patients with optic ataxia. Cereb. Cortex 15, 1561–1569.

Kwong, K.K., Belliveau, W.J., Chesler, A.D., Goldberg, E.I., Weisskoff, M.R., Poncelet, P.B., Kennedy, N.D., Hoppel, E.B., Cohen, S.M., Turner, R., 1992. Dynamic magnetic resonance imaging of human brain activity during primary sensory stimulation. PNAS 89, 5675–5679.

Lutkepohl, H., 1993. Introduction to Multiple Time Series Analysis. Springer-Verlag, New York.

Miller, E., Cohen, J., 2001. An integrative theory of prefrontal cortex function. Annu. Rev. Neurosci. 24, 167–202.

Nichols, T., Holmes, A., 2002. Nonparametric permutation tests for functional neuroimaging: a primer with examples. Hum. Brain Mapp. 15, 1–25.

Olfield, R.C., 1971. The assessments and analysis of handedness: the Edinburgh inventory. Neuropsychologia 9, 97–113.

Ombao, H., Van Bellegem, S., 2008. Evolutionary coherence of non-stationary signals. IEEE Trans. Signal Process. 56, 2259–2266.

Pollonini, L., Patidar, U., Situ, N., Rezaie, R., Papanicolaou, A.C., Zouridakis, G., 2010. Functional connectivity networks in the autistic and healthy brain assessed using Granger causality. Conf. Proc. IEEE Eng. Med. Biol. Soc. 1, 1730–1733.

Roebrock, A., Formisano, E., Goebel, R., 2005. Mapping directed influences over the brain using Granger causality and fMRI. NeuroImage 25, 230–242.

Sas Institute Inc., 2008. SAS/STAT179.2 Users Guide. Chap. 56 The MIXED Procedure. SAS Institute Inc., Cary, NC.

Schafer, J.L., Yucel, R.M., 2002. Computational strategies for multivariate mixed-effects models with missing values. J. Comput. Graph. Stat. 11, 437–457.

Shumway, H.R., Stoffer, S.D., 2006. Time series analysis and its applications. Springer texts in Statistics. .

Smith, S.M., Jenkinson, M., Woolrich, M.W., Beckmann, C.F., Behrens, T.E.J., Johansen-Berg, H., Bannister, P.R., De Luca, Marilena, Drobnjak, I., Flitney, D.E., Niazy, R.K., Saunders, J., Vickers, J., Zhang, Y., De Stefano, Nicola, Brady, J.M., Matthews, P.M., 2004. Advances in functional and structural MR image analysis and implementation as FSL. NeuroImage 23, S208–S219.

Sun, F., Miller, L., D'esposito, M., 2004. Measuring interregional functional connectivity using coherence and partial coherence analyses of fMRI data. NeuroImage 21, 647–658.

Wilson, E.R.C., Gaffan, D., Browning, F.G.P., Baxter, G.M., 2010. Functional localization within the prefrontal cortex: missing the forest for the trees? Trends Neurosci. 33, 533–540.

Worsley, K., Friston, K., 1995. Analysis of fMRI time-series revisited-again. NeuroImage 2, 173–181.

Wu, T., Wang, L., Hallett, M., Chen, Y., Li, K., Chan, P., 2010. Effective connectivity of brain networks during self-initiated movement in Parkinson's disease. NeuroImage 49 (3), 2581–2587.